CHAPTER 4

Synergistic Effect of CdSe Quantum Dots (QDs) and $PC_{61}BM$ in PCDTBT:$PC_{61}BM$:CdSe QDs Bulk Heterojunction Based Organic Solar Cells

Contents

4.1 Introduction 71

4.2 Experimental Details 72

4.2.1 Materials and Synthesis 72

4.2.2 Solar Cell Fabrication 73

4.2.3 Film and Device Characterization 75

4.3 Results and Discussion 75

4.3.1 Optical Characterization 76

4.3.2 Electrical Characterization 79

4.4 Conclusion 82

*Part of this work has been published as:

Amit Kumar et al., "Synergistic Effect of CdSe Quantum Dots (QDs) and $PC_{61}BM$ on Ambient-Air Processed ZnO QDs/PCDTBT:$PC_{61}BM$:CdSe QDs/MoO_3 Based Ternary Organic Solar Cells," *Nanotechnology*, 31, 465404, 2020.

CHAPTER 4

Synergistic Effect of CdSe Quantum Dots (QDs) and $PC_{61}BM$ in PCDTBT:$PC_{61}BM$:CdSe QDs Bulk Heterojunction Based Organic Solar Cells

4.1 Introduction

Incorporation of metallic (Au and Ag) or semiconducting (CdSe, CdS, PbSe, PbS, and Cu_2S) nanoparticles in the photoactive layers is reported to enhance the photovoltaic parameters of BHJ OSCs [131]–[135]. The blend of semiconducting nanoparticles of CdSe, CdS, PbSe, PbS, and Cu_2S with organic materials in the form of organic-inorganic hybrid nanostructures as the active layer is reported to enhance the absorption and charge transport properties of the photoactive layer in various photo detection devices [108], [136]–[138]. After investigating the performance of the PCDTBT:$PC_{61}BM$ in Chapter-2 and Chapter-3, the synergistic effect of CdSe QDs and PCDTBT:$PC_{61}BM$ on the performance of ITO/ZnO QDs/PCDTBT:$PC_{61}BM$:CdSe QDs /MoO_3/Ag based organic-inorganic solar cells structure has been investigated in the present chapter. The ZnO QDs layer is used as the ETL as in the previous chapters while the MoO_3 layer is used for the HTL in the present study. In the present study, the PQT-12 HTL layer has been replaced by MoO_3 HTL layer due to its better energy band alignment with the active layer for achievoing better hole blocking capability as compared to that obtained from the previously used PQT-12 based HTL [139]. The layout of the rest of the chapter is given below:

Section 4.2 discusses the experimental details for fabricating the ITO/ZnO QDs/PCDTBT:$PC_{61}BM$:CdSe QDs /MoO_3/Ag structured BHJ OSC. Section 4.3

provides some important results related to the electrical and optical characteristics of fabricated ITO/ZnO QDs/PCDTBT:$PC_{61}BM$:CdSe QDs /MoO_3/Ag structure BHJ OSC which includes the current-voltage characteristics, Nyquist plots, external quantum efficiency, and absorbance. Finally, Section 4.4 concludes the major observations and findings of this chapter.

4.2 Experimental Details

In this section, PCDTBT:$PC_{61}BM$:CdSe QDs based ternary BHJ organic solar cell is fabricated and analyzed the effect of CdSe QDs on the performance parameters of the device.

4.2.1 Materials and Synthesis

ZnO QDs were synthesized using the chemical route described in ref. [101]. In brief, 100 mM of zinc acetate dihydrate was dissolved in 20 ml of 2-methoxy ethanol under nitrogen environment and kept the solution at 65ºC for stirring until the solution changed to smooth milky white. Further, 100 mM of monoethanolamine (MEA), used as stabilizing reagent, was injected into the resulting solution under controlled condition. The solution was later kept at room temperature for 24 hours at the continuous stirring condition. The synthesized colloidal ZnO QDs solution was then filtered by using a 0.22 µm PVDF filter to remove the unreacted part. The synthesized ZnO QDs solution had an average particle size of ~2.87 nm. On the other hand, the kinetic growth procedure was used for the synthesis of CdSe QDs. The precursor preparation steps were used as reported in ref. [140] for quantum dots synthesis with slight modification. In brief, the stock selenium solution was made by mixing 30 mg of selenium into the mix solution consists of 5 ml of octadecene and 0.4 ml of trioctylphosphine. Further, a cadmium precursor was prepared by sum-up three

chemicals, namely 13 mg of CdO, 0.6 ml of oleic acid, and 10 ml of octadecane, respectively, in a 25 ml round bottom flask and heated till the temperature reached 225°C. At a temperature of 225°C, 1 ml of stock selenium solution was quickly injected into the prepared cadmium solution as shown in Figure 4.1. The resulting orange colour solution was then centrifuged and washed three times with ethanol to extract the CdSe QDs. Finally, extracted CdSe QDs with average particle size of ~4.58 nm were dispersed in chloroform and used for the solar cell fabrication.

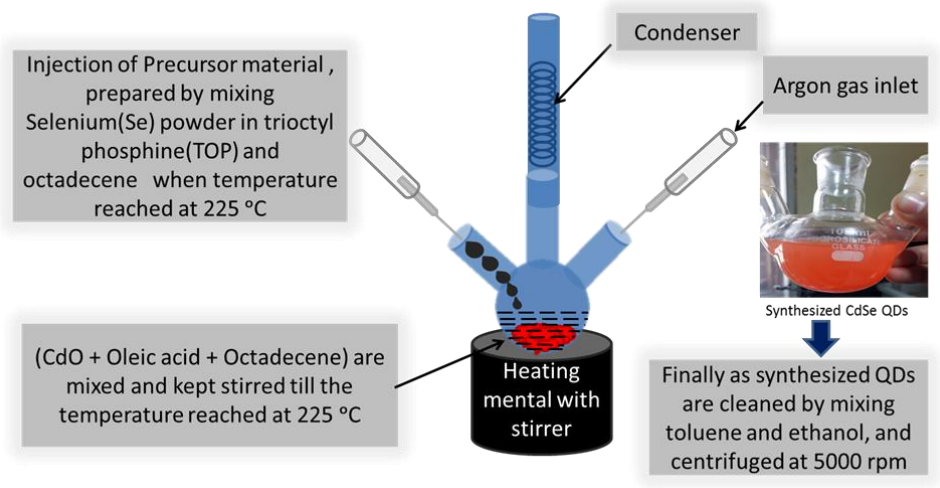

Figure 4.1: Synthesis process of CdSe QDs

4.2.2 Solar Cell Fabrication

Indium doped tin oxide (ITO) coated soda-lime glass substrates (15 × 15 mm^2) were used to fabricate the binary and ternary OSCs. The fabrication process was carried out in an ambient air atmosphere unless specific conditions are mentioned. The substrates were cleaned and dried in the oven under the flow of nitrogen gas. The ZnO QDs ETL was deposited using a spin coating technique at 2000 rpm for 40 s. The resultant film was dried at 110°C for 10 min, and this deposition was repeated multiple times to achieve a thickness of ~35 nm. Finally, the ZnO QDs film was annealed at 200°C for 30 min in an ambient air atmosphere to work efficiently as an ETL for the

OSCs. Two separate active layer solutions were prepared for the fabrication of two types of BHJ OSCs. The first active layer solution was prepared by blending p-type PCDTBT (5 mg ml^{-1}dissolved in dichlorobenzene) and n-type $PC_{61}BM$(15 mg ml^{-1}dissolved in chloroform). The solution for the second active layer was prepared by mixing 1 ml of each separate solution of PCDTBT (15 mg ml^{-1} in dichlorobenzene), $PC_{61}BM$ (30 mg ml^{-1} in chloroform), and CdSe QDs(15 mg ml^{-1} in chloroform). Initially, the solution of PCDTBT was stirred using a magnetic bead. Subsequently, the solutions of $PC_{61}BM$ and CdSe QDs were added to the solution of PCDTBT with continuous stirring for 24 h. The obtained ternary solution was well dispersed in 3 ml (20 mg ml^{-1}).

The mixing of an equivalent amount of CdSe QDs to the p-type polymer resulted in the best charge transportation [108]. Both prepared active layer solutions were continuously stirred overnight to get the evenly mixed solutions. Further, the prepared solutions were deposited upon ZnO QDs coated substrate for the identical thickness of the active layer and heated at 120°C in the oven under a nitrogen environment for 30 min. Over the active layer, an HTL layer of 10 nm thin MoO_3 was deposited using the thermal evaporation unit (FL400 SMART COAT 3.0 A from Hind High Vacuum, India) at a vacuum level of $\sim 3 \times 10^{-6}$ mbar and a constant rate of 0.1 Å s^{-1}. Finally, a circular electrode of Ag having a diameter of 2 mm and a thickness of 100 nm was deposited using a shadow masking technique inside the thermal evaporation unit. The two different types of device structures, namely binary and ternary, were fabricated as ITO/ ZnO QDs/PCDTBT:$PC_{61}BM$/MoO_3/Ag and ITO/ZnO QDs/PCDTBT:$PC_{61}BM$:CdSe QDs/MoO_3/Ag, respectively. Diagrams of the fabricated BHJ OSCs are shown in Figure 4.2.

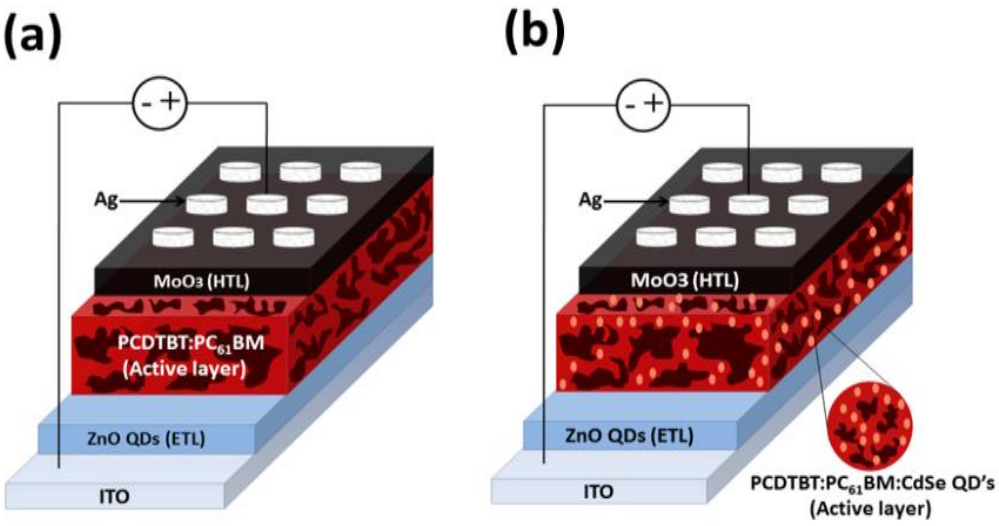

Figure 4.2: Device structure (a) Binary OSC without CdSe QDs (b) Ternary OSC with CdSe QDs.

4.2.3 Film and Device Characterization

The absorption spectra of the devices were carried out by using a UV/VIS spectrophotometer (Model V-730 from Jesco, Japan). The spectrometer (FLS 980 from Edinburgh Instruments, UK) was used to measure the photoluminescence (PL) of the devices. The semiconductor parameter analyzer (Model B1500A from Keysight, USA) was used to obtain the electrical characterization (current density vs. voltage, *J-V*). The standard 1 sunlight was obtained by using a solar simulator (Model SS50AAA, A.M. 1.5 G from Photo Emission Technology Inc., USA). Calibration of the 1 sunlight was assured by using a standard silicon reference cell (Model 60623) provided by Photo Emission Technology Inc., USA. The calculation of the external quantum efficiency (EQE) was done by using a monochromator (Model SP2150i from Princeton Instruments, USA) attached with a halogen lamp source.

4.3 Results and Discussion

In this section, the optical and electrical characteristics of fabricated

PCDTBT:$PC_{61}BM$:CdSe QDs based BHJ organic solar cell have been carried out to analyze the effect of CdSe QDs on PCDTBT:$PC_{61}BM$ based BHJ organic solar cell.

4.3.1 Optical Characterization

The effect of CdSe QDs loading in the absorption of the active layer is analyzed in the wavelength range of 350 nm to 800 nm. The absorption spectra of the ZnO QDs thin film, CdSe QDs thin film, ZnO QDs/PCDTBT:$PC_{61}BM$ stacked thin film, and ZnO QDs/PCDTBT:PC6$_1$BM:CdSe QDs stacked thin films are shown in Figure 4.3. Most of the visible spectrum passed through the ZnO QDs layer and absorbed by the active layer. The absorption in ZnO QDs/ PCDTBT:$PC_{61}BM$:CdSe QDs is slightly higher than that of ZnO QDs/ PCDTBT:$PC_{61}BM$ due to increased absorption in CdSe QDs around 515 nm shown in figure 4.3 [141]. In order to understand the charge transfer phenomena between PCDTBT and $PC_{61}BM$ by incorporating the CdSe QDs, photoluminescence (PL) characteristics have been determined in the wavelength range of 600 to 850 nm. Figure 4.4 exhibits the PL spectra of the active layer PCDTBT:$PC_{61}BM$ and PCDTBT:$PC_{61}BM$:CdSe QDs. The maximum excitation peak has been observed at 460 nm, shown in the inset of Figure 4.4. PCDTBT:$PC_{61}BM$ exhibits the maximum PL peak around 700 nm when excited at 460 nm. After mixing of CdSe QDs in the active layer, a considerable quenching of the peak around 700 nm has been observed. This quenching of the peak around 700 nm when CdSe QDs are added to PCDTBT:$PC_{61}BM$, suggests that the incorporation of CdSe QDs facilitates the improved charge transfer from PCDTBT to $PC_{61}BM$ through CdSe QDs [142].

This enhancement in the charge transfer rate could be attributed to the larger interfacial area formed when CdSe QDs have been added to the PCDTBT:$PC_{61}BM$. The energy band diagram of the binary and ternary OSCs is shown in Figure 4.5. Figure 4.5 (a) and (b) clearly show that the electrons and hole are separated efficiently towards

respective electrodes supported by ZnO QDs ETL and MoO_3 HTL. The charge transport in PCDTBT:$PC_{61}BM$ binary films occurs from PCDTBT to $PC_{61}BM$. Since the energy band levels of CdSe QDs lie in between those of PCDTBT and $PC_{61}BM$, the charge transport in PCDTBT:$PC_{61}BM$:CdSe QDs occurs through CdSe QDs as shown in Figure 4.6. The incorporation of CdSe QDs thus provides a better band alignment. As a result, the extra charge carriers generated in PCDTBT under solar light illumination are easily transported via a two-step process due to CdSe QDs as demonstrated in Figure 4.6.

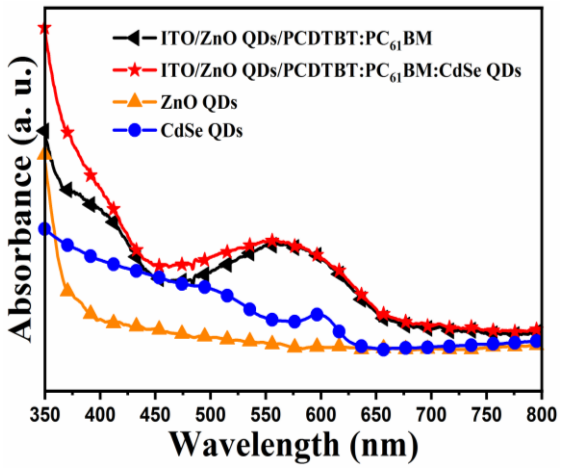

Figure 4.3: The absorbance in ZnO QDs thin film, CdSe QDs thin film, ZnO QDs/PCDTBT:$PC_{61}BM$ and, ZnO QDs/PCDTBT:$PC_{61}BM$:CdSe QDs.

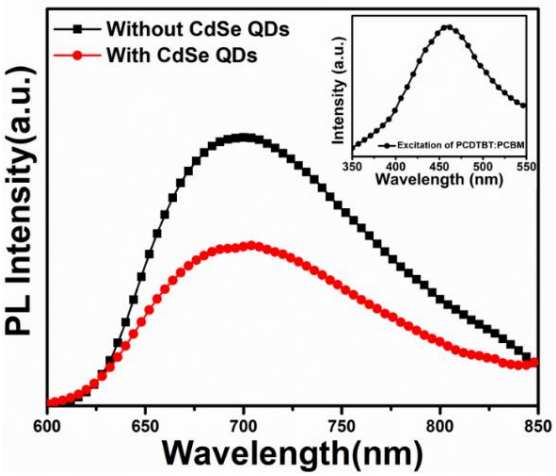

Figure 4.4: Photoluminescence (PL) spectra of PCDTBT:$PC_{61}BM$ and PCDTBT:$PC_{61}BM$:CdSe QDs.

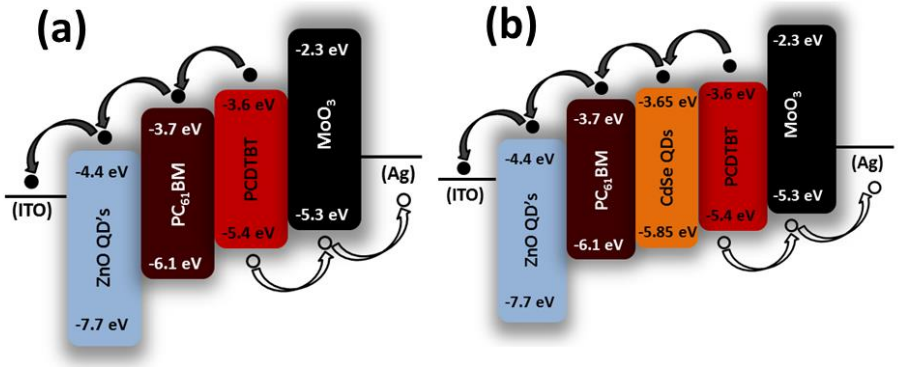

Figure 4.5: Energy band diagram (a) Binary OSC without CdSe QDs, and (b) Ternary OSC with CdSe QDs.

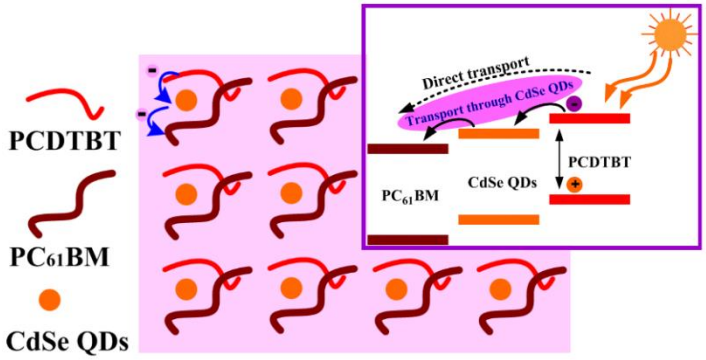

Figure 4.6: Ternary thin film made of PCDTBT, $PC_{61}BM$, and CdSe QDs. The charge carrier transport through CdSe QDs due to better band alignment.

To further understand the optical behaviour of both the OSC devices, the EQE has been plotted with respect to the wavelength ranging from 300 to 750 nm and shown in Figure 4.7. The calculation of the EQE has been completed using the relation described in [143].

$$\mathrm{EQE} = 1240 \times \left(\frac{R}{\lambda}\right) \times 100\ \% \qquad (4.1)$$

Where "R" and "λ" represent the responsivity and wavelength of the device, respectively.

Considerable enhancement has been found in the EQE of the ternary OSC (with CdSe QDs) as compared to the binary OSC (without CdSe QDs). The incorporation of CdSe

QDs in PCDTBT:$PC_{61}BM$ leads to a larger interfacial area which improves the charge transportation/extraction capability and thus improved external quantum efficiency (EQE), clearly shown in Figure 4.7.

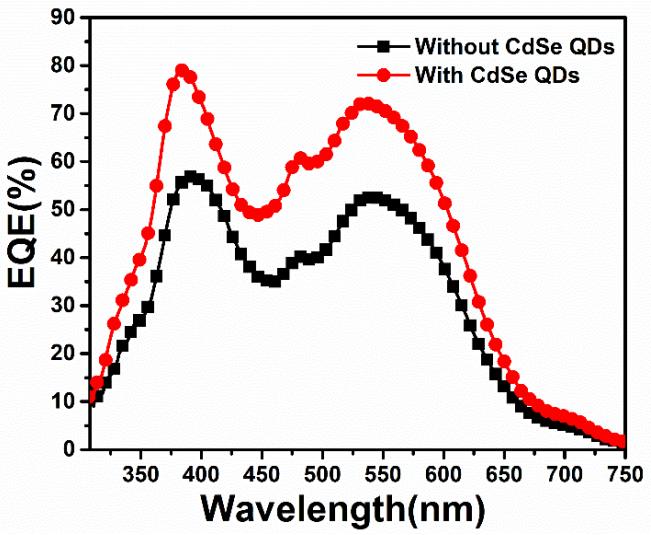

Figure 4.7: The external quantum efficiency of the fabricated binary and ternary OSC devices.

4.3.2 Electrical Characterization

To analyze the electrical behavior of the BHJ OSCs, the current density versus voltage (J-V) characteristics of both the binary and ternary OSC devices under 1 sun

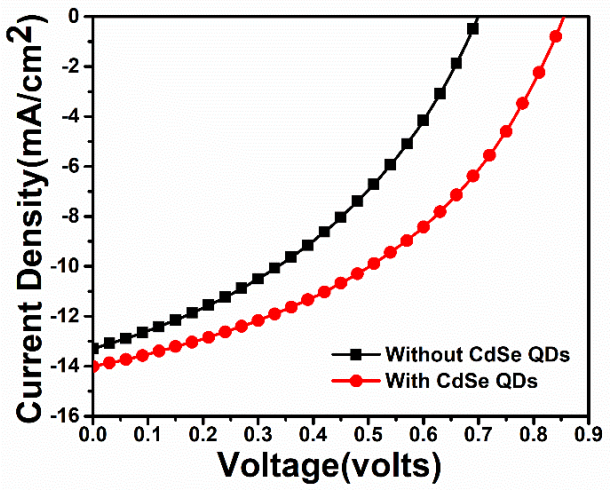

Figure 4.8: J-V characteristics of the fabricated binary and ternary OSCs.

illumination have been carried out and is shown in Figure 4.8. The calculated short

circuit current density (J_{SC}) and open-circuit voltage (V_{OC}) from the measured J-V characteristic of the binary OSC are 13.30 mA/cm^2 and 699 mV, respectively. Whereas the values of J_{SC} and V_{OC} are 14 mA/cm^2 and 854 mV for the ternary OSC. This significant enhancement in the photovoltaic parameter J_{SC} is attributed to the better charge transportation from PCDTBT to $PC_{61}BM$ via CdSe QDs in the ternary OSC [144]. We know that the V_{OC} of organic solar cells mainly depends on the energy difference (offset) between the lowest unoccupied molecular orbital (LUMO) level of the acceptor and the highest occupied molecular orbital (HOMO) level of the donor [40], [145]. Therefore, this improvement in the V_{OC} from 699 to 854 mV by the synergistic effect of CdSe QDs and $PC_{61}BM$ is due to the energy offset enhancement which could be seen clearly in the energy band diagram in Figure 4.5. All other photovoltaic parameters of the devices are detailed in table 4.1.

Table 4.1: Photovoltaic parameters of the binary and ternary OSCs.

Structure	J_{SC} (mA/cm^2)	V_{OC} (mV)	Fill Factor (FF)	PCE (%)
Binary	13.30	699	0.39	3.62
Ternary	14	854	0.42	5.02

The charge transport in the fabricated device structures has been investigated using impedance spectroscopy. Impedance spectroscopy in the frequency range of 1 kHz to 1 MHz is performed to understand the charge transportation and recombination mechanism. The Nyquist plots obtained under 1 sun illumination and operated at their open-circuit voltages for both the fabricated devices are shown in Figure 4.9. Both the devices show the semicircles, which correspond to the equivalent circuit shown in the inset of Figure 4.9. The ternary OSC shows the smaller semicircle, which implies better charge transportation from PCDTBT to the $PC_{61}BM$ via CdSe QDs is taking place.

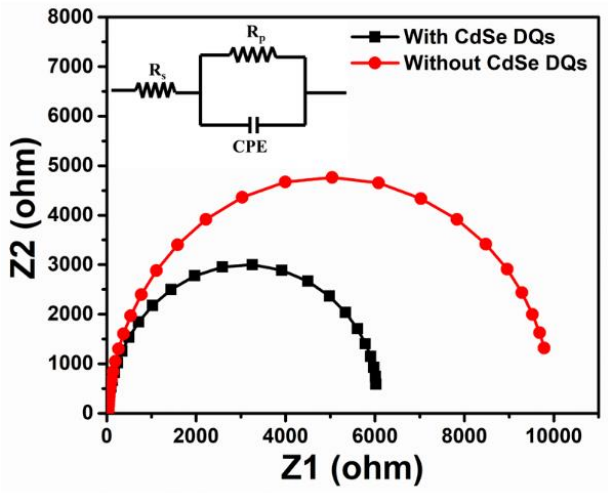

Figure 4.9: Nyquist plot of binary and ternary OSC devices under 1 sun illumination at zero applied voltage.

In order to extend some more depth of the charge transportation phenomena between donor and acceptor, the imaginary impedance Z_2 vs. frequency graph has been plotted. This plot gives an idea about the relaxation frequency of most resistive phenomena, and this relaxation frequency (fmax) is universally proportional to the relaxation time (τ) (fmax α1/ τ). Relaxation time (τ) gives an idea about the charge transfer rate between the donor and acceptor interface in the active material. The relaxation time must be as low as possible for better dissociation of excitons between donor and acceptor and thus better charge transportation [142], [146]. Figure 4.10 clearly shows that the ternary BHJ OSC exhibits a peak (relaxation frequency- fmax) shift towards the higher frequency region, which confirms that it has a lower relaxation time and thus better charge transportation as compared to the binary BHJ OSC. Now, Figure 4.11 shows the frequency-dependent real part of the impedance, which corresponds to the Rp shown in the inset of Figure 4.9. In Figure 4.11, the ternary OSC shows the lower value of impedance in the frequency ranging from 1000 to 15000 kHz compared to the binary BHJ OSC, which implies that the ternary BHJ OSC provides the better interface between donor and acceptor [146] and so better charge transportation.

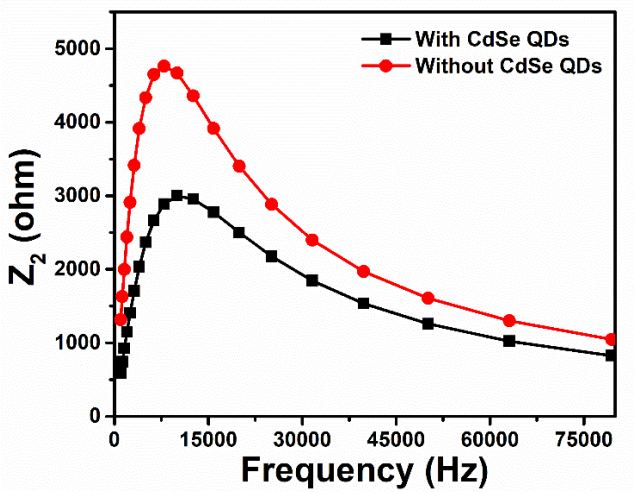

Figure 4.10: Frequency vs. imaginary part of impedance (Z_2) of the binary and ternary OSC devices.

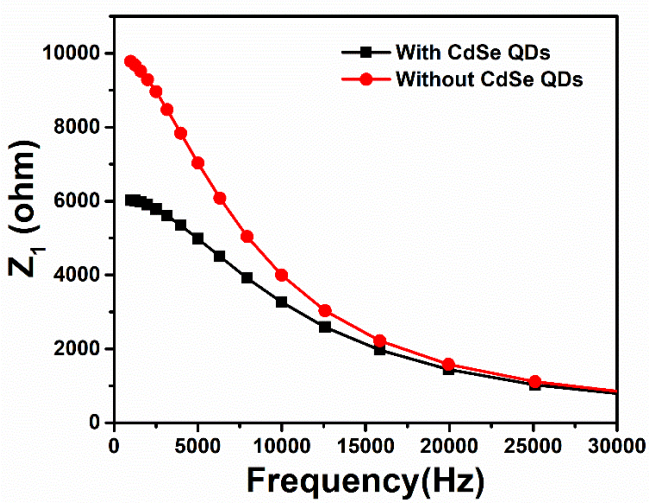

Figure 4.11: Frequency vs. real part of impedance (Z_1) of the binary and ternary OSC devices.

4.4 Conclusion

The photovoltaic performance of PCDTBT:$PC_{61}BM$ and PCDTBT:$PC_{61}BM$:CdSe QDs based binary and ternary OSCs have been investigated in this chapter. The charge transportation and photoabsorption in the photoactive thin layer of PCDTBT:$PC_{61}BM$ are tailored using the mixing of colloidal QDs of CdSe. The synergistic effect of CdSe QDs and $PC_{61}BM$ results in enhanced photoabsorption and charge transportation of the active layer of the device. The binary BHJ OSC fabricated in ITO/ZnO QDs/PCDTBT:$PC_{61}BM$/MoO3/Ag and the ternary BHJ OSC fabricated in ITO/ZnO

QDs/PCDTBT:$PC_{61}BM$:CdSe QDs/MoO3/Ag structures are characterized under the light of 1 sun. It has been found that the ternary BHJ OSC has better photovoltaic parameters compared to the binary BHJ OSC. The blending of CdSe QDs with PCDTBT:$PC_{61}BM$ improves J_{SC} from 13.30 to 14 mA/cm^2, V_{OC} from 699 to 854 mV, and the PCE from 3.62 to 5.02% due to enhanced charge transportation. The impedance measurements are used to validate the effective charge transportation in the binary and ternary BHJ OSCs.